

Taylor & Francis
Taylor & Francis Group

Molecular Physics

An International Journal at the Interface Between Chemistry and Physics

ISSN: 0026-8976 (Print) 1362-3028 (Online) Journal homepage: http://www.tandfonline.com/loi/tmph20

The PNO–MP2 gradient and its application to molecular geometry optimisations

Marius S. Frank, Gunnar Schmitz & Christof Hättig

To cite this article: Marius S. Frank, Gunnar Schmitz & Christof Hättig (2016): The PNO–MP2 gradient and its application to molecular geometry optimisations, Molecular Physics, DOI: 10.1080/00268976.2016.1263762

To link to this article: http://dx.doi.org/10.1080/00268976.2016.1263762

Published online: 21 Dec 2016.

Submit your article to this journal

View related articles

View Crossmark data

Full Terms & Conditions of access and use can be found at
http://www.tandfonline.com/action/journalInformation?journalCode=tmph20

Download by: [Ruhr-Universitat Bochum Universitaetsbibliothek] **Date:** 22 December 2016, At: 04:41

MOLECULAR PHYSICS, 2016
http://dx.doi.org/10.1080/00268976.2016.1263762

Taylor & Francis
Taylor & Francis Group

RESEARCH ARTICLE

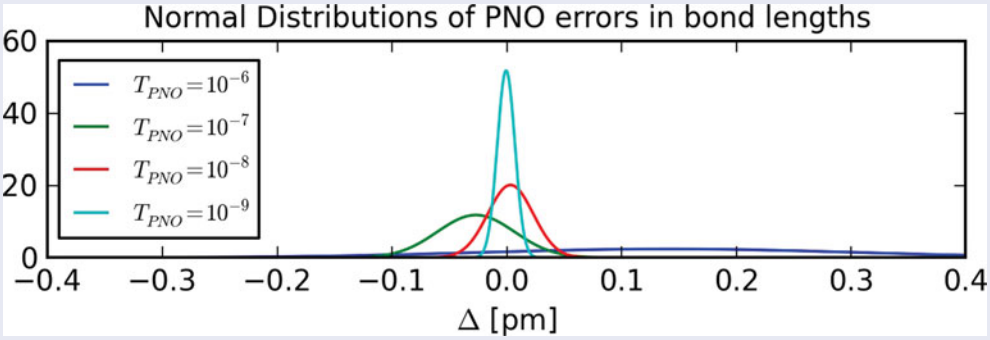
The PNO–MP2 gradient and its application to molecular geometry optimisations

Marius S. Frank[a], Gunnar Schmitz[b] and Christof Hättig[a]

[a]Lehrstuhl für Theoretische Chemie, Ruhr-Universität Bochum, Bochum, Germany; [b]Deparment of Chemistry, Aarhus University, Aarhus C, Denmark

ABSTRACT

A preliminary implementation of a gradient for MP2 based on the pair natural orbital approximation (PNO–MP2) is presented. The accuracy of the PNO approximation for geometries is investigated by comparing bond lengths and bond angles of the PNO–MP2 structures with results from canonical MP2. Special emphasis is put on the optimisation of weakly bound complexes, such as differently sized water clusters. It is found that the error introduced by the PNO approximation is already for moderate PNO thresholds negligible compared to the inherent error of MP2. However, too loose PNO thresholds lead to convergence difficulties in geometry optimisations. This is observed in particular for floppy groups as, for example, methyl groups with low rotational barriers. Compared to optimisations with canonical MP2, the convergence thresholds have to be mainly energy and less coordinate based to comply with the slight roughness of the potential energy surface which is introduced by the PNO selection.



ARTICLE HISTORY
Received 7 September 2016
Accepted 11 November 2016

KEYWORDS
Local MP2; PNO–MP2 gradient; geometry optimisations; accuracy

1. Introduction

One of the major challenges of modern quantum chemistry is to find highly accurate and systematically improvable methods for the calculation of energies, geometries and properties, which are applicable to large molecular systems. This is due to the fact that well-established canonical methods, which are known to be very precise, show a steep scaling of the computational costs with the system size $\mathcal{N}$. Hence, canonical post-Hartree–Fock (HF) wave function methods are restricted to small- or medium-sized systems.

Fortunately, new approaches to reduce the cost-scaling of wave function methods came up during the past decade. Most methods that aim at a reduced scaling are based on the fact that the dynamical electron correlation is a short-range effect. These methods are called local correlation methods. Many local correlation methods aim to achieve a truncation of the virtual space, while performing the calculation on the whole molecule. There exist different schemes for the truncation of the virtual space. The maybe most popular and refined one was originally developed by Saebø and Pulay [1–6] and later extended and implemented by Werner and coworkers [7–11]. According to the ideas of Saebø and Pulay, the virtual orbital space is spanned by projected atomic orbitals (PAOs), which differ from the AOs only from orthogonalisation tails introduced by the projection onto the virtual space. Using this approach, Schütz and Werner succeeded in implementing linear scaling local versions of MP2 [7,8], CCSD [9–14] and CCSD(T) [13–17]. Although these methods have a low cost-scaling, a major drawback is that the local domains need to be specified prior to a calculation, what results in a limited error control. Furthermore, the local domains soon

CONTACT Marius S. Frank Marius.Frank@rub.de
© 2016 Informa UK Limited, trading as Taylor & Francis Group

become very large for highly accurate calculations, which then diminishes the computational savings obtained by the PAO approach.

Pair natural orbital (PNO) methods, which were originally pioneered in the 1970s by Meyer [18–21], Ahlrichs, Kutzelnigg, Staemmler and co-workers [22–24], can be used to circumvent this issue, but they are also computationally more demanding. Recognising that the most severe bottleneck of these methods (the integral transformations) can be avoided by the use of the resolution-of-the-identity (RI) approximation [25,26] led Neese and coworkers to the revival of the PNO approach [27–32] for closed-shell as well as for high-spin open-shell molecules. PNOs, in contrast to PAOs, are pair specific and lead to a very compact representation of the virtual space. Typically, 30–40 PNOs per pair are on average sufficient [33]. Another advantage of PNOs is that they are constructed from an (approximate) correlated wave function and thereby they adapt themselves automatically to the specific requirements of the molecular system. The error of a PNO calculation can be controlled systematically by adjusting one single threshold, T_{PNO}, which truncates the PNO expansion.

A compromise between PAOs and PNOs has been proposed by Yang and co-workers [33]. They introduced orbital-specific virtuals (OSVs), which are not pair-specific, but orbital-specific virtual orbitals. The computational costs of the construction and integral transformation of OSVs lie in between those of the PAOs and PNOs. Yang et al. have successfully applied the OSV approach to the MP2 and CCSD [33] methods and were able to carry out calculations with up to 2334 basis functions at the CCSD level.

Hättig and co-workers as well as Werner and coworkers combined the compactness of the PNO approach with the lower integral transformation costs of OSVs within a hybrid OSV–PNO–MP2 approach [34,35]. They first construct OSVs and subsequently generate the PNOs in the already truncated space spanned by the OSVs, which results in a $\mathcal{O}(\mathcal{N}^4)$-scaling of the PNO construction. The scaling of this hybrid method could further be reduced to $\mathcal{O}(\mathcal{N}^3)$ by replacing the time-determining step – the construction of the OSVs through a full diagonalisation of the doubles amplitude matrices – by an iterative block Davidson algorithm [36]. These methods have successfully been applied to PNO excited-state calculations with the approximate coupled cluster singles and doubles model CC2 [37] and the extended algebraic-diagrammatic construction through second order ADC(2)-x [38], and the explicitly correlated methods MP2-F12 [34,39,40], MP3-F12 [34] and CCSD[F12] [41].

Furthermore, Neese and co-workers reported near-linear scaling implementations of CCSD [32] and CCSD(T) [42]. This was achieved by combining the PAO and PNO approaches: the PNOs are expanded in PAOs, which belong to pair-specific domains. These domain-based local PNO (DLPNO) approaches have been applied to calculations with more than 8800 basis functions. Similar techniques (combination of PAOs, OSVs and PNOs) led Werner and co-workers to the development of (parallel) algorithms, which show a linear scaling in the molecular size and a near-inverse scaling in the number of processors, for MP2 [43] and MP2-F12 [44]. More recently, Neese and co-workers introduced the concept of sparse maps, which is based on the sparse representation of tensors [45]. Using this formalism, they succeeded in the implementation of a linear scaling algorithm for DLPNO–CCSD(T), which could be applied to calculations with more than 20,000 basis functions and 1000 atoms [46].

Due to the fact that PNOs produce smooth potential energy surfaces [29], the next natural step is to investigate how well PNOs perform in geometry optimisations. This is the aim of the present work. The following text is structured as follows: after a brief review of the conventional MP2 Lagrangian and the PNO theory in Section 2, the implementation of the PNO–MP2 gradient is presented. In Section 4, we apply the PNO–MP2 gradient to Baker's test set for geometry optimisations. The errors in the PNO–MP2 geometries relative to the canonical geometries are investigated based on a statistical analysis for the bond lengths and angles. Section 5 deals with the optimisation of different water clusters in order to investigate the accuracy of PNO–MP2 in the description of weak intermolecular interactions. Finally, in Section 6, the performance of the implementation is investigated, and in Section 7, the findings are summarised and an outlook on future work is given.

2. Theory and implementation

2.1. The conventional RI–MP2 gradient

For MP2, the (orbital-relaxed) Lagrange function is given by

$$\mathcal{L}^{\mathrm{MP2}} = \langle \mathrm{HF}|H + [H, T_2]|\mathrm{HF}\rangle + \sum_{\mu_2} \bar{t}_{\mu_2} \langle \mu_2|H + [F, T_2]|\mathrm{HF}\rangle + \sum_{\mu_0} \bar{\kappa}_{\mu_0} F_{\mu_0}, \tag{1}$$

where the operators F and H denote the Fock and Hamilton operators and $T_2 = \sum_{\mu_2} t_{\mu_2} \tau_{\mu_2}$ the cluster operator. The index μ_2 runs over double replacements. In this work, we assume closed-shell systems and use the spin-free operators [47] $\tau_{aibj} = E_{ai}E_{bj}$ and $\bar{t}^{ij}_{ab} = 4t^{ij}_{ab} - 2t^{ji}_{ab}$.

Here and in the following, we use the convention that indices $a, b, c, \ldots$ denote active virtual molecular orbitals (MOs) and $i, j, k, \ldots$ active occupied MOs *(in the frozen core approximation)*. General MOs will be labelled with $p, q, r, \ldots$ and atomic orbitals (AOs) with $\mu, \nu, \kappa, \ldots$. To denote the complete, i.e. active + inactive, virtual and occupied MO subspace we use, respectively, the capital letters A, B and I, J. The HF reference determinant $|\mathrm{HF}\rangle$ is parametrised as

$$|\mathrm{HF}\rangle = \exp\left(\sum_{\mu_0} \kappa_{\mu_0}(E_{\mu_0} - E^{\dagger}_{\mu_0})\right)|\mathrm{HF}_0\rangle, \tag{2}$$

where $|\mathrm{HF}_0\rangle$ is chosen such that the orbital rotation parameters κ_{μ_0} vanish for the unperturbed system. The first term in Equation (1) corresponds to the total MP2 energy. The second term accounts for the MP2 amplitude equations, while the last term includes a sum over the Fock matrix elements which are required to vanish. The index range of μ_0 depends on the constraints applied to the Fock operator. Here, we use a non-canonical condition and only require that the Fock matrix is block-diagonal in the occupied/virtual and active/inactive subblocks.

After some rearrangements the RI–MP2 Lagrangian can be written as

$$\mathcal{L}^{\mathrm{MP2}} = \frac{1}{2}\sum_{pq} D^{\mathrm{SCF}}_{pq} h_{pq} + \sum_{pq}\left(\frac{1}{2}D^{\mathrm{SCF}}_{pq} + D^{\mathrm{MP2}}_{pq} + \bar{\kappa}_{pq}\right)F_{pq} + \frac{1}{2}\sum_{aibj} d^{nsep}_{aibj}(ai|bj)^{\mathrm{RI}} \tag{3}$$

with the SCF and the unrelaxed MP2 one-particle densities, D^{SCF}_{pq} and D^{MP2}_{pq}, the non-separable part of the two-electron density d^{nsep}_{aibj} and the one-electron (core) Hamiltonian matrix h_{pq}. Explicit expressions for the densities can be found, e.g. in Ref. [48]. The two-electron repulsion integrals $(ai|bj)^{\mathrm{RI}}$ are evaluated within the RI approximation:

$$(ai|bj)^{\mathrm{RI}} = \sum_{Q} C_{Qbj}(Q|ai), \tag{4}$$

with

$$C_{Qbj} = \sum_{P}(P|bj)\left[\mathbf{V}^{-1}\right]_{PQ}, \tag{5}$$

and the Coulomb metric

$$V_{PQ} = (P|Q). \tag{6}$$

Here, and in the following, capital indices $P, Q, R, \ldots$ denote auxiliary basis functions and $(Q|ai)$ and $(P|Q)$ are three- and two-index electron repulsion integrals.

2.2. Pair natural orbitals

PNOs are defined as linear combination of virtual orbitals

$$|\bar{a}\rangle = \sum_{a}|a\rangle d^{ij}_{a\bar{a}}, \tag{7}$$

with the expansion coefficient $d^{ij}_{a\bar{a}}$ chosen such that they diagonalise the contribution D^{ij}_{ab} of the pair ij to an one-electron density matrix [49]

$$\sum_{ab} d^{ij}_{a\bar{a}} D^{ij}_{ab} d^{ij}_{b\bar{b}} = \delta_{\bar{a}\bar{b}} n^{ij}_{\bar{a}}. \tag{8}$$

For D^{ij}_{ab}, we choose the MP2 density which is given by

$$D^{ij}_{ab} = 2\sum_{c}\left(u^{ij}_{ac}t^{ij}_{bc} + u^{ij}_{ca}t^{ij}_{cb}\right), \tag{9}$$

with

$$u^{ij}_{ab} = 2t^{ij}_{ab} - t^{ij}_{ba}. \tag{10}$$

The PNO coefficients are obtained by diagonalising D^{ij}_{ab} in a quasi-canonical pair-specific basis $\{\tilde{a}_{ij}\}$, which is obtained by merging and orthonormalising the OSV sets of i and j: first, the OSV coefficients $d^{ii}_{a\tilde{a}_i}$ (which are equal to the PNO coefficients of a diagonal pair) are determined by solving the OSV eigenvalue problem

$$\sum_{b} D^{ii}_{ab} d^{ii}_{b\tilde{a}_i} = n_{\tilde{a}_i} d^{ii}_{a\tilde{a}_i} \tag{11}$$

iteratively. For details, we refer to Ref. [36]. After building the aforementioned quasi-canonical pair-specific basis, the PNO coefficients are obtained by solving the PNO equations in this basis:

$$\sum_{\tilde{a}_{ij}\tilde{b}_{ij}} d^{ij}_{\tilde{a}_{ij}\bar{a}_{ij}} D^{ij}_{\tilde{a}_{ij}\tilde{b}_{ij}} d^{ij}_{\tilde{b}_{ij}\bar{b}_{ij}} = \delta_{\bar{a}_{ij}\bar{b}_{ij}} n^{ij}_{\bar{a}_{ij}} \tag{12}$$

The approximate amplitudes are then calculated as

$$t^{ij}_{\tilde{a}_{ij}\tilde{b}_{ij}} = \frac{(\tilde{a}_{ij}i|\tilde{b}_{ij}j)}{F_{ii} - \epsilon_{\tilde{a}_{ij}} + F_{jj} - \epsilon_{\tilde{b}_{ij}}}, \tag{13}$$

where F_{ii} are the diagonal elements of the (non-diagonal) Fock matrix in the localised molecular orbital (LMO)

basis and $\epsilon_{\tilde{a}_{ij}}$ the eigenvalues of the Fock matrix (diagonalised) in the unified OSV space. The eigenvalues $n^{ij}_{\tilde{a}}$ of D^{ij}_{ab} are the natural occupation numbers. When sorted in descending order, these natural occupation numbers decrease rapidly to zero if i and j are LMOs.

2.3. Lagrange multipliers for localised orbitals

2.3.1. The localisation constraint

In a truncated PNO basis or if LMO pairs are neglected, the wave function is no longer invariant under rotations among the occupied MOs. To account for this, the Lagrangian in Equation (3) needs to be augmented with a localisation constraint. In the current work for Forster-Boys [50] localisation, we get

$$\left(\frac{d}{d\lambda_{kl}}\sum_{i,j}\left(\langle\tilde{i}|\vec{r}|\tilde{i}\rangle-\langle\tilde{j}|\vec{r}|\tilde{j}\rangle\right)^2\right)_{\lambda=0}=0. \tag{14}$$

The perturbed LMOs $\tilde{\phi}_i$ are obtained from the unperturbed LMOs ϕ_i by the unitary transformation

$$\tilde{\phi}_i=\exp\left(\sum_{i<j}\lambda_{ij}\left(E_{ij}-E_{ji}\right)\right)\phi_i. \tag{15}$$

The antisymmetric matrix $\boldsymbol{\lambda}$ describes the change of the localisation coefficients with respect to an external perturbation, similar to the matrix $\boldsymbol{\kappa}$, which describes the change of the MO coefficients with respect to the perturbation (vide infra). Evaluation of Equation (14) yields

$$0=(\langle i|\vec{r}|i\rangle-\langle j|\vec{r}|j\rangle)\langle j|\vec{r}|i\rangle=B_{ij}. \tag{16}$$

Thus, the Lagrangian becomes

$$\mathcal{L}^{\mathrm{MP2}}=\frac{1}{2}\sum_{pq}D^{\mathrm{SCF}}_{pq}h_{pq}+\sum_{pq}\left(\frac{1}{2}D^{\mathrm{SCF}}_{pq}+D^{\mathrm{MP2}}_{pq}+\bar{\kappa}_{pq}\right)F_{pq}+\frac{1}{2}\sum_{aibj}d^{nsep}_{aibj}(ai|bj)^{\mathrm{RI}}+\sum_{i<j}\bar{\lambda}_{ij}B_{ij}. \tag{17}$$

In principle, additional constraints that take the selection of the PNOs into account would have to be considered. In the current work, we neglect these constraints since their effect on the gradient and the final geometries can be expected to be of similar size as the noise due to the geometry dependence of the PNO selection.

Furthermore, it should at this point be mentioned that we do not take the gradient of the pair correction (evaluated in the OSV basis $\{\tilde{a}_i\}$)

$$\mathcal{E}_{ij}=c_{OS}(1+\delta_{ij})\sum_{\tilde{a}_i\tilde{b}_j}\frac{2K^{ij}_{\tilde{a}_i\tilde{b}_j}K^{ij}_{\tilde{a}_i\tilde{b}_j}}{F_{ii}-F_{\tilde{a}_i\tilde{a}_i}+F_{jj}-F_{\tilde{b}_j\tilde{b}_j}} \tag{18}$$

with $K^{ij}_{\tilde{a}_i\tilde{b}_j}=(\tilde{a}_i i|\tilde{b}_j j)$ and the diagonal elements of the (non-diagonal) Fock matrix evaluated in the OSV basis into account in our preliminary implementation. For the calculation of energies, the above equation is used to screen the pair list and subsequently these estimated pair correlation energies of discarded pairs are added to the total energy. For further details, it is referred to Refs. [34,36].

2.3.2. The coupled–perturbed Hartree–Fock and localisation equations

Now that a suitable Lagrangian has been set up, the Lagrange multipliers can be determined. The matrix $\bar{\boldsymbol{\kappa}}$, whose only non-vanishing blocks are the virtual/occupied and inactive/active blocks, is then obtained by solving the so-called Z-vector equations [51]. For the virtual/occupied block, they can be written as

$$\sum_{BJ}\bar{\kappa}_{BJ}\left(\delta_{JI}F_{BA}-\delta_{BA}F_{IJ}+\frac{1}{2}A_{BJAI}\right)=-\eta^{\kappa}_{AI}, \tag{19}$$

with the Z-CPHF matrix $A_{pqrs}=4(pq|rs)^{\mathrm{RI}}-(pr|sq)^{\mathrm{RI}}-(ps|rq)^{\mathrm{RI}}$, which also is evaluated using the RI approximation (see Section 2.4 for details), and the right-hand side (RHS) vector

$$\eta^{\kappa}_{AI}=L_{IA}-L^{''}_{AI}+M_{AI}+\frac{1}{2}\sum_{pq}\left(D^{\mathrm{MP2}}_{pq}+\bar{\kappa}^{OO}_{pq}\right)A_{pqIA}. \tag{20}$$

The intermediate M_{AI} stems from the differentiation of the localisation constraint and has non-vanishing elements only if I is an active occupied orbital:

$$M_{qi}=\sum_{w=xyz}\sum_{l}\bar{\lambda}_{il}\Big[\langle i|r_w|q\rangle\langle l|r_w|i\rangle+\frac{1}{2}(\langle i|r_w|i\rangle-\langle l|r_w|l\rangle)\langle l|r_w|q\rangle\Big]. \tag{21}$$

The intermediates L_{IA} and $L^{''}_{AI}$, which contain contractions with the non-separable part of the two-electron density (i.e. the doubles amplitudes), are evaluated in the PNO basis as follows:

$$L''_{aq} = \sum_{\mu} C_{\mu q} \sum_{ij} \sum_{\bar{a}} d^{ij}_{a\bar{a}} \sum_{P} (\mu i|P) \Gamma^{ij}_{P,\bar{a}i}, \tag{22}$$

$$L_{iq} = \sum_{\nu} C_{\nu q} \sum_{j} \sum_{P\mu} (\mu\nu|P) \sum_{\bar{a}} C^{ij}_{\mu\bar{a}} \Gamma^{ij}_{P,\bar{a}i}, \tag{23}$$

with

$$\Gamma^{ij}_{P,\bar{a}i} = \sum_{\bar{b}j} t^{ij}_{\bar{a}\bar{b}} C^{ij}_{P,\bar{b}j}, \tag{24}$$

$$C^{ij}_{P,\bar{b}j} = \sum_{\mu} C_{P,\mu,j} C^{ij}_{\mu\bar{b}}, \tag{25}$$

and the coefficients $C^{ij}_{\mu\bar{b}} = \sum_b C_{\mu b} d^{ij}_{b\bar{b}}$, which transform from the AO to the PNO space of pair *ij*.

Furthermore, the unrelaxed MP2 density also needs to be evaluated from the amplitudes in the PNO basis. For the virtual/virtual block, this can be done straightforwardly as

$$D^{\mathrm{MP2}}_{ab} = 2 \sum_{ij} \sum_{\bar{a}\bar{b}} d^{ij}_{a\bar{a}} d^{ij}_{b\bar{b}} \sum_{\bar{c}} u^{ij}_{\bar{a}\bar{c}} t^{ij}_{\bar{b}\bar{c}}. \tag{26}$$

For the occupied/occupied block, additional transformations with PNO overlap matrices appear:

$$D^{\mathrm{MP2}}_{ij} = -2 \sum_{k\bar{a}_{jk}\bar{b}_{jk}} u^{jk}_{\bar{a}_{jk}\bar{b}_{jk}} \sum_{\bar{c}_{ik}} S^{ik,jk}_{\bar{c}_{ik}\bar{b}_{jk}} \sum_{\bar{d}_{ik}} S^{ik,jk}_{\bar{d}_{ik}\bar{a}_{jk}} t^{ik}_{\bar{d}_{ik}\bar{c}_{ik}}. \tag{27}$$

The overlap of PNOs belonging to different pairs *ik* and *jk* is defined as

$$S^{ik,jk}_{\bar{a}\bar{b}} = \sum_{c} d^{ik}_{c\bar{a}} d^{jk}_{c\bar{b}}. \tag{28}$$

The matrix $\bar{\kappa}^{OO}_{pq}$ in Equation (20) contains the inactive-occupied/active-occupied block of $\bar{\boldsymbol{\kappa}}$. These Lagrange multipliers are determined by

$$\sum_{K} \left(\bar{\kappa}_{KJ} F_{KI} - \bar{\kappa}_{IK} F_{JK} \right) = -(L_{IJ} + M_{IJ}) \tag{29}$$

The Lagrange multipliers $\bar{\lambda}_{ij}$ are determined by the condition that the Lagrangian has to be stationary with respect to variations of the localisation parameters λ_{ij}. This leads to the coupled–perturbed localisation (Z-CPL) equations [52]:

$$\left(1 - \hat{P}_{kl}\right) \sum_{w=xyz} \sum_{i} \bar{\lambda}_{ki} \Big[\langle k|r_w|l\rangle \langle i|r_w|k\rangle + \frac{1}{2} \left(\langle k|r_w|k\rangle - \langle i|r_w|i\rangle \right) \langle i|r_w|l\rangle \Big] = -\theta_{kl} \tag{30}$$

with the usual permutation operator $\hat{P}_{kl} f_{kl} = f_{lk}$ and the RHS vector

$$\theta_{kl} = (1 - \hat{P}_{kl}) \sum_{i} \left(D^{\mathrm{MP2}}_{il} F_{ik} + \frac{1}{2} L_{lk} \right) \tag{31}$$

Since the Lagrange multipliers $\bar{\boldsymbol{\kappa}}$ do not contribute to the Z-CPL equations, the latter equations can be solved prior to the Z-CPHF equations.

2.4. The PNO–MP2 gradient

Now, that the Lagrange multipliers have been determined, the gradient can be evaluated in the AO basis as follows:

$$\begin{aligned} \left(\frac{d\mathcal{L}^{\mathrm{MP2}}}{dx} \right)_{x=0} = & \sum_{\mu\nu} D^{\mathrm{eff}}_{\mu\nu} h^{[x]}_{\mu\nu} - \sum_{\mu\nu} F^{\mathrm{eff}}_{\mu\nu} S^{[x]}_{\mu\nu} \\ & + \sum_{Q\mu\nu} \Delta_{Q,\mu\nu} (Q|\mu\nu)^{[x]} \\ & + \sum_{PQ} \gamma_{PQ} (P|Q)^{[x]} + \sum_{Q'\mu\nu} \Delta^{\mathrm{SCF}}_{Q',\mu\nu} (Q'|\mu\nu)^{[x]} \\ & + \sum_{P'Q'} \gamma^{\mathrm{SCF}}_{P'Q'} (P'|Q')^{[x]} \\ & + \sum_{w\in\{xyz\}} \sum_{\mu\nu} D^{(w)}_{\mu\nu} \langle \mu|r_w|\nu\rangle^{[x]} \end{aligned} \tag{32}$$

where *P*, *Q* denote auxiliary basis functions for the correlation part and *P*′, *Q*′ auxiliary basis functions for the RI–JK approximation [53] used in the HF part.

The effective Fock matrix $F^{\mathrm{eff}}_{\mu\nu}$, also known as energy-weighted density matrix, is defined as

$$\begin{aligned} F^{\mathrm{eff}}_{\mu\nu} = & \sum_{pq} C_{\mu p} C_{\nu q} \sum_{u} D^{\mathrm{eff}}_{pu} F_{qu} \\ & + \frac{1}{2} \sum_{Iq} C_{\mu I} C_{\nu q} \sum_{rs} \left(D^{\mathrm{MP2}}_{rs} + \bar{\kappa}_{rs} \right) A_{rsIq} \\ & + \frac{1}{2} \sum_{pq} C_{\mu p} C_{\nu q} \left(L_{pq} + L''_{pq} \right) + \sum_{Ij} C_{\mu I} C_{\nu j} M_{Ij} \end{aligned} \tag{33}$$

with the usual relaxed one-electron density $D^{\mathrm{eff}}_{\mu\nu} = D^{\mathrm{SCF}}_{\mu\nu} + D^{\mathrm{MP2}}_{\mu\nu} + \bar{\kappa}_{\mu\nu}$. The three- and two-index two-particle densities for the correlation part are defined as [54]

$$\gamma_{PQ} = \sum_{i\mu} C_{P,\mu i} \Gamma_{Q,\mu i}, \tag{34}$$

$$\Delta_{Q,\mu\nu} = \sum_{i} \Gamma_{Q,\mu i} C_{\nu i}.$$

Table 1. Definition of the three- and two-index two-electron densities $\Delta^{\mathrm{SCF}}_{Q,\mu\nu}$ and $\gamma^{\mathrm{SCF}}_{PQ}$ for the SCF part of the gradient.

$$\Delta^{\mathrm{SCF}}_{Q,\mu\nu} = \left(D^{\mathrm{MP2}}_{\mu\nu} + \bar{\kappa}_{\mu\nu}\right) i^{\mathrm{SCF}}_{Q} + 2\sum_{I} \tilde{\Gamma}^{\mathrm{SCF}}_{Q,\nu I} C_{\mu I}$$
$$\gamma^{\mathrm{SCF}}_{PQ} = \sum_{\mu I} \Gamma^{\mathrm{SCF}}_{P,\mu I} C_{Q,\mu I}$$
$$\tilde{\Gamma}^{\mathrm{SCF}}_{Q,\nu I} = C_{\nu I} i^{\mathrm{eff}}_{Q} - \sum_{\mu}\left(\tfrac{1}{2} D^{\mathrm{SCF}}_{\mu\nu} + D^{\mathrm{MP2}}_{\mu\nu} + \bar{\kappa}_{\mu\nu}\right) C_{Q,\mu I}$$
$$\Gamma^{\mathrm{SCF}}_{Q,\mu I} = 2C_{\mu I}\left(i^{\mathrm{eff}}_{Q} - i^{\mathrm{SCF}}_{Q}\right) - \sum_{\nu}\left(\tfrac{1}{2} D^{\mathrm{SCF}}_{\nu\mu} + D^{\mathrm{MP2}}_{\nu\mu} + \bar{\kappa}_{\nu\mu}\right) C_{Q,\nu I}$$
$$i^{\mathrm{SCF}}_{Q} = \sum_{\mu\nu} D^{\mathrm{SCF}}_{\mu\nu} C_{Q,\mu\nu} = \sum_{\mu I} C_{Q,\mu I} C_{\mu I}$$
$$i^{\mathrm{eff}}_{Q} = \sum_{\mu\nu} D^{\mathrm{eff}}_{\mu\nu} C_{Q,\mu\nu} = i^{\mathrm{SCF}}_{Q} + \sum_{P} j^{\mathrm{MP2}}_{P} \left[\mathbf{V}^{-1}\right]_{PQ} + \sum_{IA\mu} C_{\mu A} \bar{\kappa}_{AI} C_{Q,\mu I}$$
$$j^{\mathrm{MP2}}_{Q} = \sum_{\mu\nu} (\mu\nu|Q) \sum_{pq} C_{\mu p} C_{\nu q} \tilde{D}^{\mathrm{MP2}}_{pq}$$

Table 2. Geometry convergence thresholds used for the RI– and PNO–MP2 geometry optimisations.

	RI–MP2	PNO–MP2
$T_{\Delta E}$	1×10^{-6}	1×10^{-6}
$T_{\mathrm{RMS(G)}}$	5×10^{-4}	5×10^{-4}
T_{MaxG}	1×10^{-3}	1×10^{-3}
T_{RMSD}	5×10^{-4}	5×10^{-3}
T_{MaxD}	1×10^{-3}	2×10^{-2}

The definition of the three- and two-electron densities ($\Delta^{\mathrm{SCF}}_{Q,\mu\nu}$ and $\gamma^{\mathrm{SCF}}_{PQ}$) for the SCF part are summarised in Table 1. The last term in Equation (32) is the contribution from the localisation constraint with the density $D^{(w)}_{\mu\nu}$, which is defined as

$$D^{(w)}_{\mu\nu} = \sum_{kl} C_{\mu k} C_{\nu l} \bar{\lambda}_{kl} [\langle k|r_w|k\rangle + \langle l|r_w|k\rangle]. \tag{35}$$

This term is a direct consequence of the use of Boys localisation (in the localisation constraint). Since it only involves contractions with sparse one-electron integrals, the computational costs are insignificant compared to the overall costs for computing the gradient.

3. Computational details

The PNO–MP2 gradient has been implemented in a development version of the TURBOMOLE quantum chemistry program package [55,56]. The SCF calculations have been done with the ridft [53,57–60] and reference MP2 calculations with the ricc2 [48,61,62] program. For the geometry optimisations, the optimiser statpt, which is part of TURBOMOLE, was used. During the geometry optimisations, five convergence criteria have been tested: the energy change ($T_{\Delta E}$); the root-mean-square displacement of the atoms (T_{RMSD}); the maximum displacement of the atoms (T_{MaxD}); the RMS of the gradient (T_{RMSG}) and the maximum component of the gradient (T_{MaxG}). Table 2 summarises the different thresholds for PNO– and RI–MP2 geometry optimisations.

The thresholds for the displacements were increased for PNO–MP2 geometry optimisations compared to the defaults. This accounts for the fact that the PNO approximation and the neglect of the PNO equations as constraint in the Lagrangian hinder such tight convergence of the geometry as it is default for the statpt program (see also Section 4.1 for details).

Table 3. The molecules included in the Baker test set for geometry optimisations and the individual bonds with the corresponding labels considered for the calculation of the deviations shown in Figure 1.

Molecule	Bond	Label	Molecule
Dimethylpentane	C–C	1	Water
Naphthalene	C=C	2	Ammonia
Acetylene	C ≡ C	3	Ethane
Allene	C=C	4	Ethanol
Benzidine	C–C	5	Methylamine
1,3,5-Trisilacyclohexane	Si–C	6	Benzene
Disilyl ether	Si–O	7	Acetone
ACANIL01	N–CO	8	Benzaldehyde
Caffeine	N–CO	9	1,3-Difluorobenzene
Histidine	N=C	10	1,3,5-Trifluorobenzene
2-Hydroxybicyclopentane	C–O	11	Neopentane
Menthone	C=O	12	Furan
Mesityl oxide	C=O	13	ACHTAR10
Difluropyrazine	O–C	14	Pterin
1,5-Difluoronaphthalene	C–F	15	
Hydrosulphane	S–O	16	

The actual (PNO-)MP2 geometry optimisations have been carried out using the def2-SVP [63,64], def2-TZVPP [64], def2-QZVPP [64,65], aug-cc-pVTZ and aug-cc-pVQZ [66–68] orbital basis sets and the corresponding auxiliary basis sets for RI-MP2 [69,70] and RI-JK [53,60]. Furthermore, the frozen core approximation has been used in all calculations.

4. Results

4.1. Application of PNO–MP2 to Baker's test set for geometry optimisations

For the investigation of the convergence behaviour and the accuracy of PNO–MP2 geometries in a broad variety of bonding situations, we use Baker's test set for geometry optimisations [71]. The molecules included in this test set are listed in Table 3.

The errors introduced by the PNO approximation are investigated as function of the PNO threshold ($T_{\mathrm{PNO}} = 10^{-6} \ldots 10^{-9}$) and the basis set size (def2-SVP, def2-TZVPP, def2-QZVPP). As statistical measures, we use the mean error $\bar{\Delta}$, mean absolute error $\bar{\Delta}^{\mathrm{abs}}$, maximum error Δ^{max} and the standard deviation σ.

For these statistical measures of the errors in bond lengths and angles, each covalent bond (angle) in all molecules has been considered: first, the statistical measures have been calculated for each molecule and, subsequently, these molecule-specific statistical data have

then been used to obtain the statistical data over the whole test set.

4.1.1. Bond lengths

Before considering the statistical measures, which are calculated over the whole test set, it is interesting to investigate how the errors introduced by the PNO approximation behave for different bonding situations. For this purpose, characteristic bonds in a subset of molecules have been selected (see Table 3). The errors of PNO–MP2 in these bond lengths in the def2-QZVPP basis set are shown in Figure 1.

From this figure, it is obvious that the errors usually decrease with decreasing PNO thresholds. But this observation does not hold for all cases. For example, the error in the C=C bond in allene slightly increases from $T_{\mathrm{PNO}} = 10^{-6}$ to $T_{\mathrm{PNO}} = 10^{-8}$ and only decreases by further lowering the PNO threshold. A similar behaviour can be seen for the error in the C ≡ C bond in acetylene. Here, the error significantly increases by about 0.45 pm going from $T_{\mathrm{PNO}} = 10^{-6}$ to $T_{\mathrm{PNO}} = 10^{-7}$. This non-monotonic behaviour is a result of the superposition of errors with different sign. But compared to the MP2 intrinsic errors (typical and maximum errors of 0.46 and 1.70 pm for the first-row elements [47,72] (in the cc-pCVQZ basis) and 0.71 and 3.49 pm (in the cc-pCVQZ basis) for the second-row elements [73], respectively), this effect is small.

Table 4. Statistical measures of errors in bond lengths (pm).

T_{PNO}		def2-SVP	def2-TZVPP	def2-QZVPP
10^{-6}	$\bar{\Delta}$	−0.03	0.14	0.03
	$\bar{\Delta}^{\mathrm{abs}}$	0.05	0.46	0.17
	$\bar{\Delta}^{\mathrm{max}}$	0.46	2.26	0.63
	σ	0.01	0.16	0.11
10^{-7}	$\bar{\Delta}$	$\lvert\bar{\Delta}\rvert < 0.01$	−0.03	0.12
	$\bar{\Delta}^{\mathrm{abs}}$	0.01	0.06	0.17
	$\bar{\Delta}^{\mathrm{max}}$	0.12	0.61	0.52
	σ	<0.01	0.03	0.12
10^{-8}	$\bar{\Delta}$	$\lvert\bar{\Delta}\rvert < 0.01$	$\lvert\bar{\Delta}\rvert < 0.01$	0.06
	$\bar{\Delta}^{\mathrm{abs}}$	<0.01	0.03	0.07
	$\bar{\Delta}^{\mathrm{max}}$	0.04	0.20	0.40
	σ	<0.01	0.02	0.02
10^{-9}	$\bar{\Delta}$	$\lvert\bar{\Delta}\rvert < 0.01$	$\lvert\bar{\Delta}\rvert < 0.01$	0.04
	$\bar{\Delta}^{\mathrm{abs}}$	<0.01	0.01	0.06
	$\bar{\Delta}^{\mathrm{max}}$	0.04	0.10	0.30
	σ	<0.01	<0.01	0.02

The statistical measures are shown in Figure 2 and Table 4. From the mean errors, it can be seen that there is no systematic trend concerning overestimation or underestimation of bond lengths with respect to RI–MP2 in the small def2-SVP basis, while in the larger triple-ζ and quadruple-ζ basis sets, the PNO results tend to overestimate bond lengths, as it is expected as a consequence of the partial neglect of dynamic correlation. The mean absolute and maximum errors, in contrast, systematically

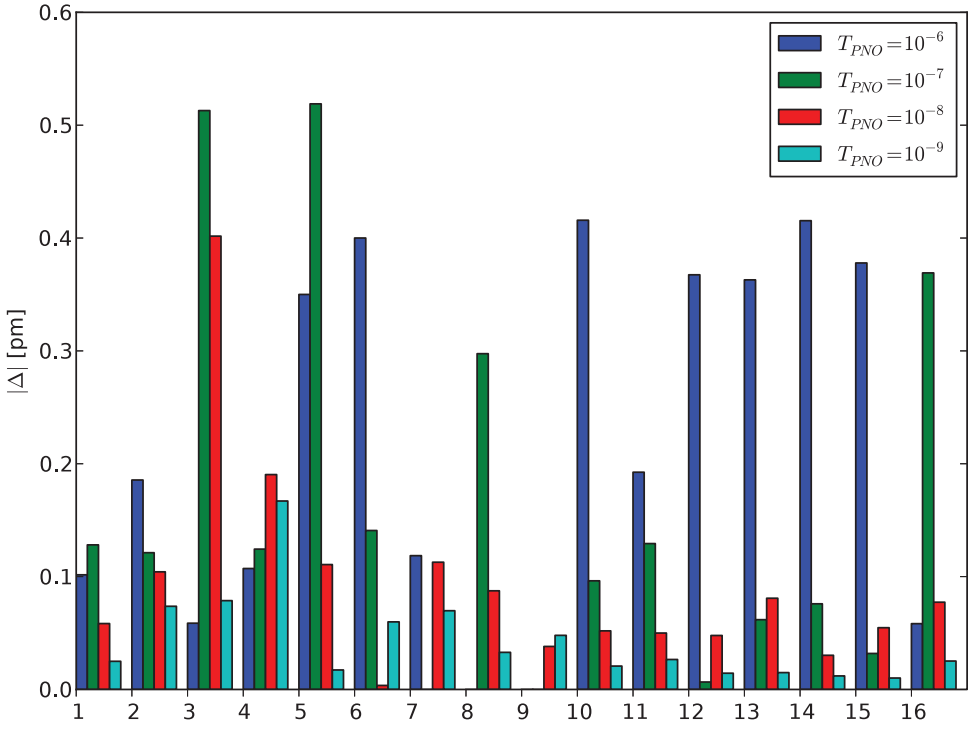


Figure 1. Errors in individual bonds in the def2-QZVPP basis set. The numbers on the *x*-axis refer to the numbering of molecules/bonds in Table 3.

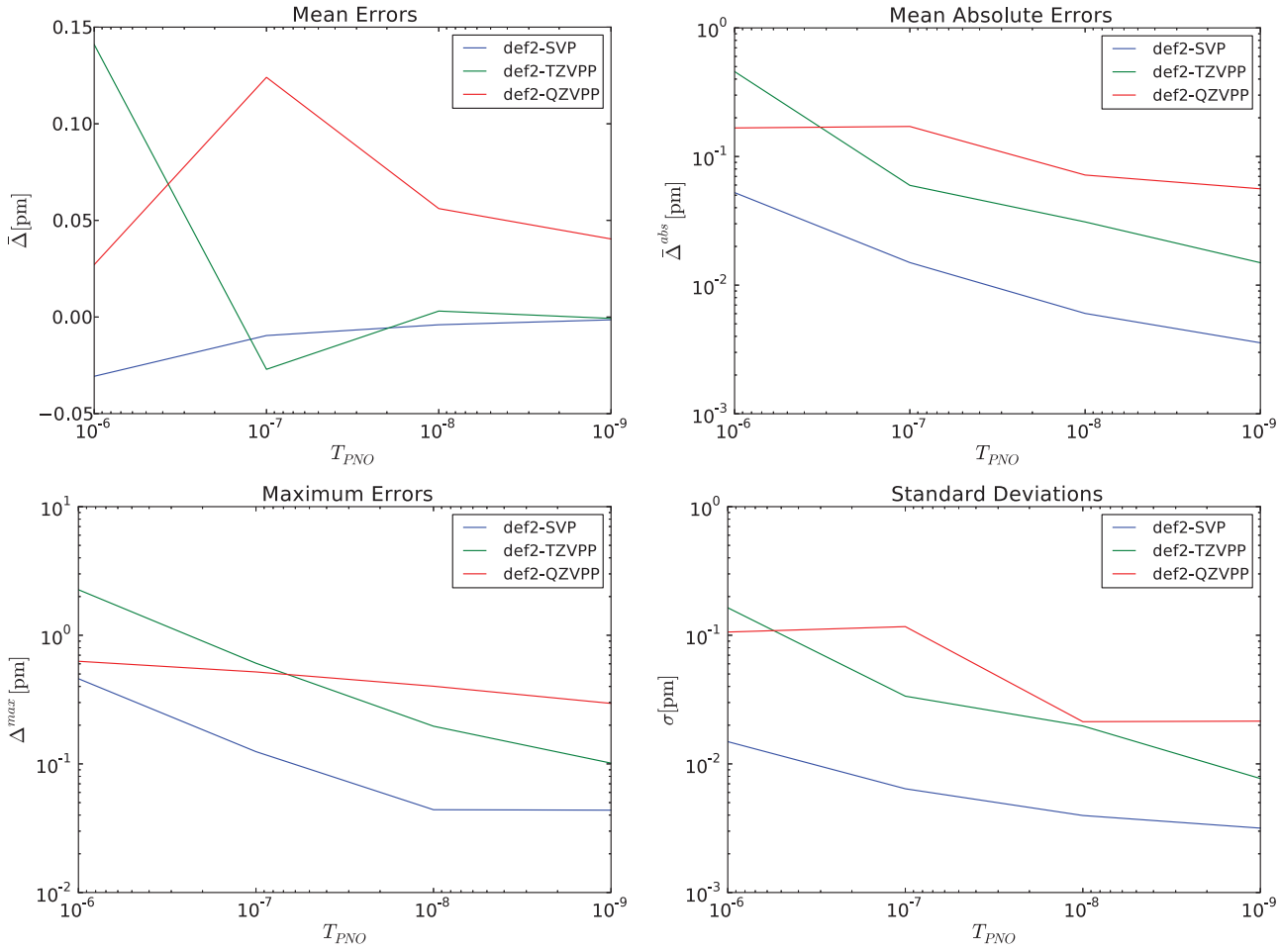


Figure 2. Graphical visualisation of the statistical measures obtained for the errors in bond lengths.

decrease for tighter PNO thresholds. Already for $T_{\mathrm{PNO}} = 10^{-6}$, both of these measures are below the respective MP2 intrinsic errors observed by Helgaker and co-workers [47] for the first-row elements (with one exception for the maximum error with $T_{\mathrm{PNO}} = 10^{-6}$ in def2-TZVPP). In addition, the mean absolute and maximum errors increase in most cases with the size of the basis set. This is reasonable, since the virtual space increases with the basis set size. This then leads to a more truncated virtual space if the same PNO threshold is applied for a calculation in a larger basis set. But compared to the MP2 intrinsic errors, this effect is small.

To better understand the origin of the relatively large maximum error of 2.26 pm with $T_{\mathrm{PNO}} = 10^{-6}$ in the def2-TZVPP basis, we analysed the structure of benzidine where this error occurs. The problematic bond is the C–C bond that connects the two phenyl rings. A competition between steric repulsion and dispersion interactions leads at the MP2 level to a dihedral angle between the phenyl rings of around 142° and a bond length of 147 pm (see also Table 5). With $T_{\mathrm{PNO}} = 10^{-6}$ and the def2-TZVPP basis, the truncation of the virtual space apparently is too harsh to capture the dispersion interaction accurately enough and the geometry optimisation converges to an almost perpendicular structure.

Table 5. Comparison of the RI–MP2 and the PNO–MP2 C–C bond length and the dihedral angle between the two phenyl groups in benzidine.

	Dihedral angle (°)		C–C bond length (pm)	
	def2-TZVPP	def2-QZVPP	def2-TZVPP	def2-QZVPP
$T_{\mathrm{PNO}} = 10^{-6}$	92.6	138.4	149.4	147.3
$T_{\mathrm{PNO}} = 10^{-7}$	143.8	145.7	147.7	147.5
$T_{\mathrm{PNO}} = 10^{-8}$	143.2	141.3	147.3	147.1
$T_{\mathrm{PNO}} = 10^{-9}$	142.3	140.6	147.2	147.0
RI–MP2	142.0	142.0	147.1	147.0

The normal distributions shown in Figure 3 give a nice overview of the observations made so far. While being rather narrow and minimally displaced in the def2-SVP basis set for all PNO thresholds studied, they are broader for the larger basis sets. The curves become more sharply peaked with decreasing PNO thresholds, indicating the expected convergence towards the canonical results.

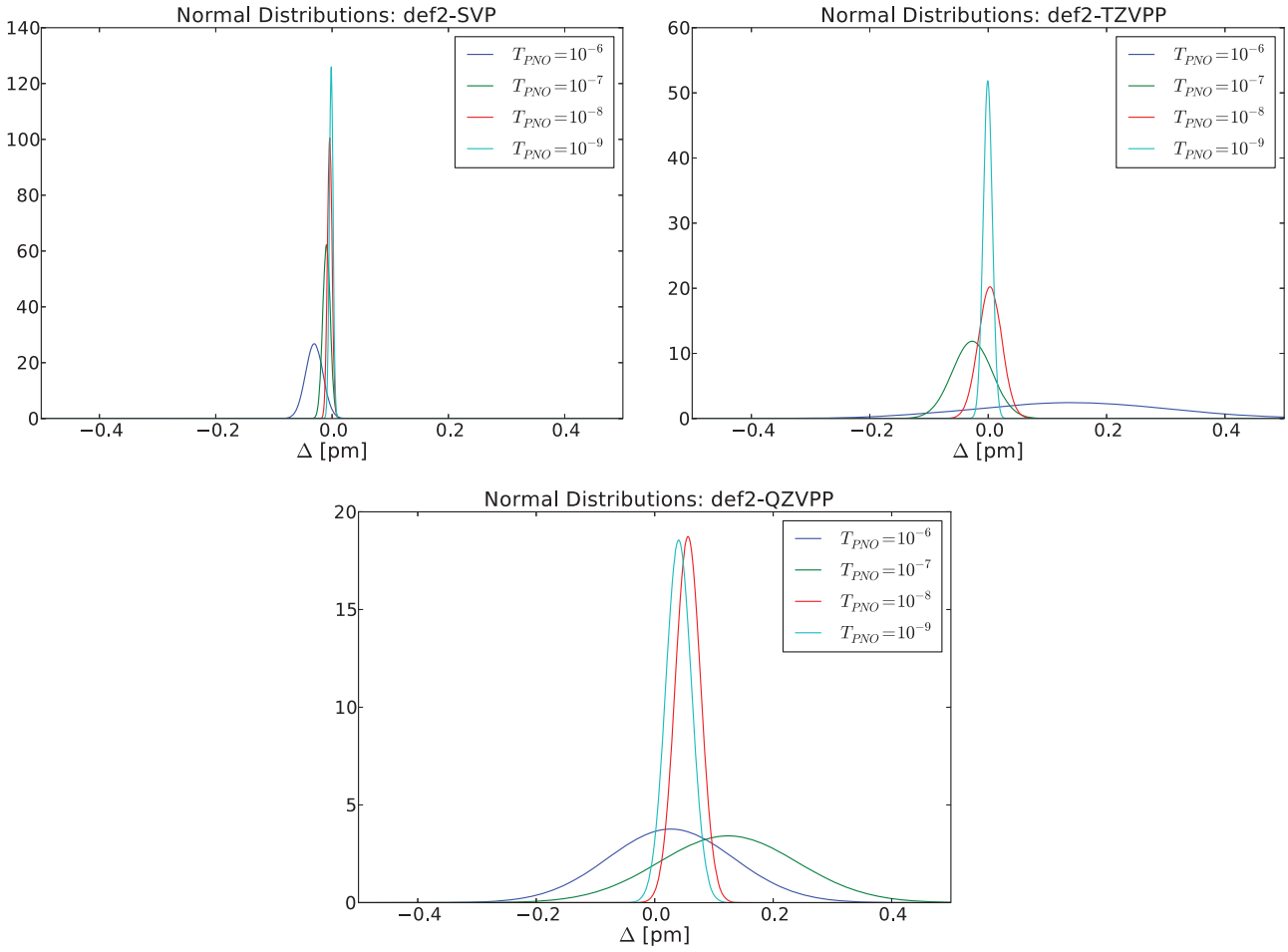


Figure 3. Normal distributions of the PNO errors (in bond lengths) in different basis sets.

Furthermore, it is important to mention at this point that even though the statistical measures for $T_{\mathrm{PNO}} = 10^{-6}$ and $T_{\mathrm{PNO}} = 10^{-7}$ overall look promising (even for $T_{\mathrm{PNO}} = 10^{-6}$ about 99.9% of the errors lie within the MP2 error bar), for a few molecules and basis set sets; however, the optimisations did not convergence within the thresholds defined in Table 2. This was the case for pterin ($T_{\mathrm{PNO}} = 10^{-6}$) and caffeine ($T_{\mathrm{PNO}} = 10^{-6}$ and $T_{\mathrm{PNO}} = 10^{-7}$) in all basis sets. Additionally, disilyl ether could not be converged for $T_{\mathrm{PNO}} = 10^{-6}$ in def2-TZVPP and for $T_{\mathrm{PNO}} = 10^{-7}$ in def2-QZVPP and ACANIL01 could not be converged for $T_{\mathrm{PNO}} = 10^{-6}$ in def2-QZVPP. Caffeine, ACANIL01 and disilyl ether are rather floppy molecules (especially due to the methyl groups) with many local minima on a flat potential energy surface. For these molecules, the rotation of the methyl groups prevents the energy or the gradient from convergence: after an initial decrease of the energy, the optimisation starts to oscillate. Similar observations have been made for pterin. It is, however, unclear whether this is a problem of the PNO approximation itself or of the neglect of the PNO equations as constraints in the Lagrangian in the current preliminary implementation.

Table 6. Statistical measures of errors in bond angles (°).

T_{PNO}		def2-SVP	def2-TZVPP	def2-QZVPP
10^{-6}	$\bar{\Delta}^{\mathrm{abs}}$	0.04	0.15	0.17
	$\bar{\Delta}^{\mathrm{max}}$	0.51	1.30	4.57
	σ	0.04	0.06	0.29
10^{-7}	$\bar{\Delta}^{\mathrm{abs}}$	0.02	0.07	0.18
	$\bar{\Delta}^{\mathrm{max}}$	0.54	0.56	0.79
	σ	0.03	0.03	0.10
10^{-8}	$\bar{\Delta}^{\mathrm{abs}}$	0.01	0.05	0.09
	$\bar{\Delta}^{\mathrm{max}}$	0.39	0.48	0.44
	σ	0.02	0.03	0.13
10^{-9}	$\bar{\Delta}^{\mathrm{abs}}$	0.01	0.02	0.05
	$\bar{\Delta}^{\mathrm{max}}$	0.38	0.18	0.50
	σ	0.02	0.05	0.04

4.1.2. Bond angles

Statistical measures for the errors in bond angles are given in Figure 4 and Table 6. They have been evaluated in a similar way as the bond lengths before. For the

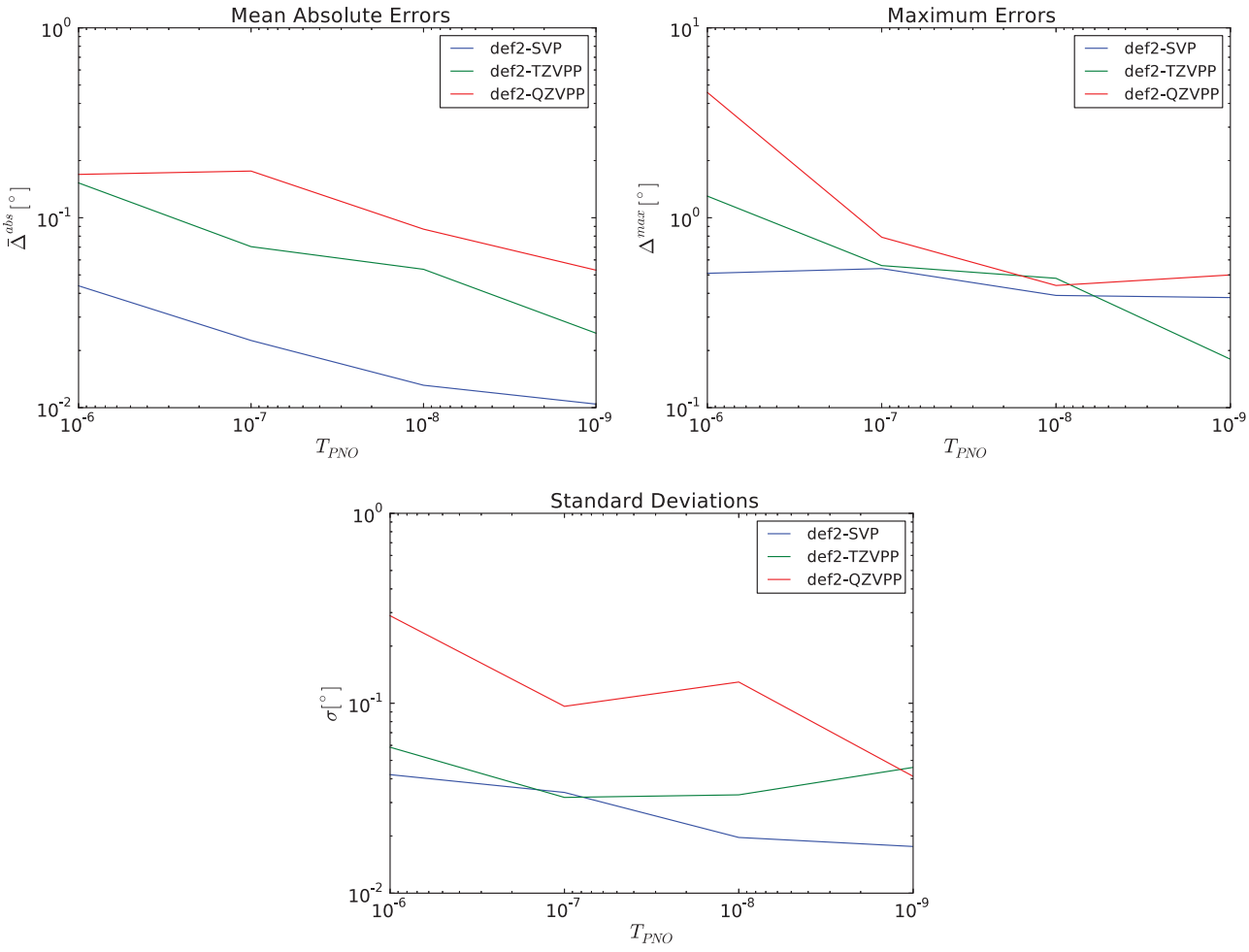


Figure 4. Graphical visualisation of the statistical measures obtained for the errors in bond angles.

angles we present, however, no results for the mean error, since the errors in individual angles tend to cancel each other, as, for example, for the three bond angles at a sp^2 hybridised central atom. All in all, the curves show a similar behaviour as the ones for the bond lengths. Again, the mean absolute errors are below the MP2 intrinsic errors (0.19° for first-row elements [47,72] and 0.12° for second-row elements [73]) in every case. The maximum error at $T_{\mathrm{PNO}} = 10^{-6}$ and $T_{\mathrm{PNO}} = 10^{-9}$ in the def2-QZVPP basis both occur in the Si–O–Si bond of disilyl ether. The large error at $T_{\mathrm{PNO}} = 10^{-6}$ and the significant decrease at $T_{\mathrm{PNO}} = 10^{-9}$ suggest that somewhat tighter thresholds should be used for molecules containing second-row elements, even though the errors in the bond lengths are small.

4.2. The structure of water clusters

One of the key areas, where MP2 or related double-hybrid DFT functionals are applied, are geometry optimisations of molecular clusters and complexes, with geometries that are vastly determined by weak interactions, as e.g. hydrogen bonding. To investigate the accuracy of PNO–MP2 on such intermolecular complexes, different water hexamers and octamers have been optimised.

The error between canonical and PNO–MP2 in the nearest-neighbour O–O distances has been used as a measure for the description of hydrogen bonds, since these are also commonly used measures to describe water complexes in the literature [74–76] (see Table 7). Furthermore, the errors in H–O–H, O–H···O and H···O–H(···O) have been been analysed (see Table 8) to obtain a more complete overview of the similarity of the structures. The same statistical measures as described above have been used. But in this case, the statistical measures have been evaluated by averaging only over the errors at each water cluster to obtain a more complete overview of the similarity of the structures.

As a general trend, it can be seen from Tables 7 and 8 that the errors in the aug-cc-pVQZ basis set are somewhat larger than those in the aug-cc-pVTZ basis for the same PNO threshold. Similar to the observations made for

Table 7. Statistical measures for the errors in the nearest-neighbour O–O distances (pm) in different water clusters. The errors were obtained by comparing the results for canonical and PNO–MP2 results without counterpoise correction.

		aug-cc-pVTZ					aug-cc-pVQZ				
		$(H_2O)_6$			$(H_2O)_8$		$(H_2O)_6$			$(H_2O)_8$	
T_{PNO}		Prism	Cage	Book	D_{2d}	S_4	Prism	Cage	Book	D_{2d}	S_4
10^{-6}	$\bar{\Delta}$	5.05	4.66	4.75	5.72	5.51	9.32	10.12	–[a]	11.87	–[b]
	$\bar{\Delta}^{abs}$	5.05	4.66	4.75	5.72	5.51	9.32	10.12	–[a]	11.87	–[b]
	$\bar{\Delta}^{max}$	6.58	8.44	6.53	5.95	5.75	12.91	14.52	–[a]	15.10	–[b]
	σ	1.19	1.60	0.91	0.16	0.31	2.83	2.08	–[a]	1.53	–[b]
10^{-7}	$\bar{\Delta}$	−0.44	−0.50	0.23	0.08	0.34	1.25	0.98	1.66	0.44	0.42
	$\bar{\Delta}^{abs}$	0.88	0.98	0.44	0.52	0.62	1.30	1.38	1.66	0.44	0.83
	$\bar{\Delta}^{max}$	1.89	1.64	0.93	0.66	0.94	5.17	2.65	2.84	0.52	1.10
	σ	0.96	0.96	0.46	0.52	0.55	1.60	1.30	0.63	0.06	0.74
10^{-8}	$\bar{\Delta}$	0.13	−0.25	−0.25	0.12	$\lvert\bar{\Delta}\rvert < 0.01$	−0.93	−0.96	−0.85	−2.60	−2.54
	$\bar{\Delta}^{abs}$	0.72	0.50	0.36	0.13	0.43	1.18	1.00	0.85	2.60	2.54
	$\bar{\Delta}^{max}$	2.92	1.36	0.61	0.27	0.82	2.70	2.32	1.46	2.70	2.71
	σ	1.10	0.59	0.32	0.11	0.47	1.06	0.70	0.41	0.07	0.09
10^{-9}	$\bar{\Delta}$	0.23	0.15	0.15	0.28	0.19	−0.43	−0.12	−0.66	−0.54	−0.63
	$\bar{\Delta}^{abs}$	0.40	0.16	0.23	0.28	0.21	1.09	0.61	0.68	0.54	0.63
	$\bar{\Delta}^{max}$	0.87	0.35	0.38	0.36	0.37	2.81	1.33	1.21	0.91	1.00
	σ	0.41	0.13	0.21	0.06	0.13	1.24	0.68	0.38	0.25	0.27
MP2[c]	$\bar{\Delta}$	−2.50	−2.48	−2.54	−2.55	−2.56	−1.30	−1.36	−1.42	−1.36	−1.36
	$\bar{\Delta}^{abs}$	2.50	2.48	2.54	2.55	2.56	1.30	1.36	1.42	1.36	1.36
	$\bar{\Delta}^{max}$	2.91	3.08	2.83	2.61	2.67	1.42	1.55	1.51	1.38	1.39
	σ	0.26	0.25	0.14	0.07	0.11	0.07	0.09	0.05	0.02	0.01

[a]No reasonable geometry found.
[b]No convergence achieved.
[c]Refers to the deviations between MP2 and CP-corrected MP2 structures.

Baker's test set, we observe that for tight PNO thresholds, i.e. $T_{PNO} = 10^{-8}$ and $T_{PNO} = 10^{-9}$, the O–O distances converge in the quadruple-zeta basis set from below.

Furthermore, it was found that the influence of basis set superposition error (BSSE) on PNO–MP2 and canonical MP2 geometries is similar for practically relevant PNO thresholds (see below). Similar observations can be made by comparing the counterpoise-corrected (CP-corrected) [77] and uncorrected MP2 and PNO–MP2 binding energies (Table 9). Hence, only the errors referring to the uncorrected results will be discussed in the following.

Table 8. Statistical measures for the errors in intermolecular and intramolecular bond angles of different water clusters. All possible H–O–H, O–H···O and H···O–H(···O) angles (°) have been included in the analysis to give a more complete overview over the similarities of the structures.

		aug-cc-pVTZ					aug-cc-pVQZ				
		$(H_2O)_6$			$(H_2O)_8$		$(H_2O)_6$			$(H_2O)_8$	
T_{PNO}		Prism	Cage	Book	D_{2d}	S_4	Prism	Cage	Book	D_{2d}	S_4
10^{-6}	$\bar{\Delta}^{abs}$	1.44	2.33	1.76	2.84	2.52	2.61	1.72	–[a]	3.14	–[b]
	$\bar{\Delta}^{max}$	4.54	9.67	3.83	4.34	3.93	17.25	5.91	–[a]	13.90	–[b]
10^{-7}	$\bar{\Delta}^{abs}$	0.68	0.75	0.74	0.78	0.92	1.61	1.70	1.67	3.80	3.43
	$\bar{\Delta}^{max}$	1.97	1.67	1.61	1.37	1.95	4.56	3.56	9.01	5.89	7.54
10^{-8}	$\bar{\Delta}^{abs}$	0.71	0.47	0.46	0.23	0.37	0.68	0.80	0.63	0.42	0.47
	$\bar{\Delta}^{max}$	2.19	1.32	2.20	0.67	1.36	3.96	2.37	1.70	0.84	1.48
10^{-9}	$\bar{\Delta}^{abs}$	0.22	0.26	0.24	0.13	0.12	0.76	0.61	0.51	0.76	0.75
	$\bar{\Delta}^{max}$	1.12	1.48	1.64	0.39	0.47	2.97	1.67	2.14	1.27	1.31
MP2[c]	$\bar{\Delta}^{abs}$	0.26	0.27	0.34	0.22	0.23	0.11	0.12	0.13	0.09	0.10
	$\bar{\Delta}^{max}$	0.67	0.64	1.22	0.36	0.42	0.25	0.31	0.33	0.19	0.25

[a]No reasonable geometry found.
[b]No convergence achieved.
[c]Refers to the deviations between MP2 and CP-corrected MP2 structures.

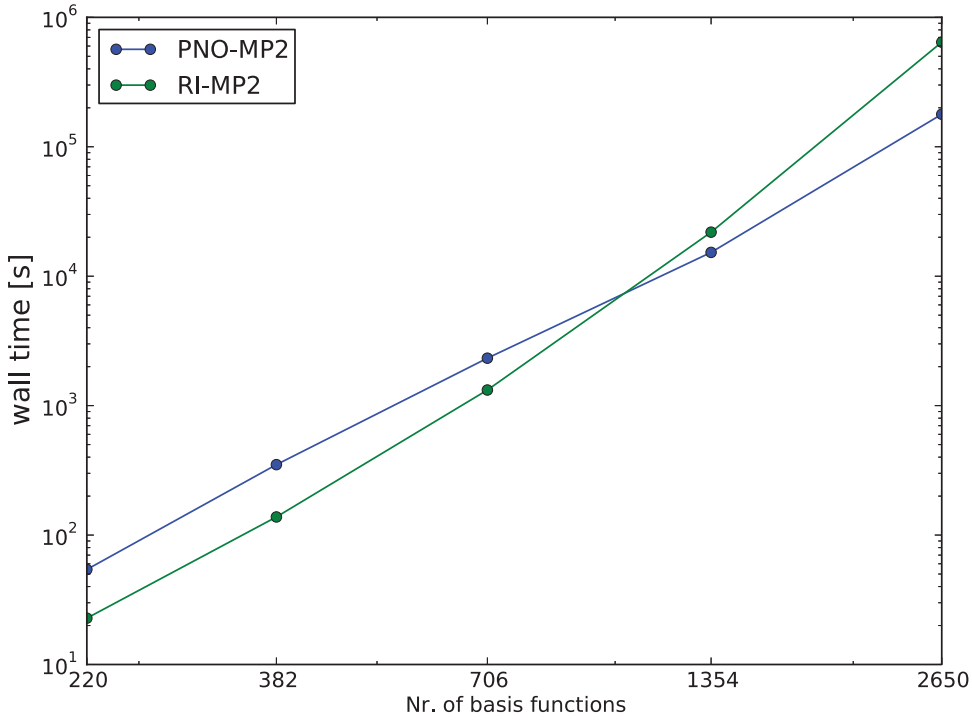


Figure 5. Comparison of the performance of canonical RI-MP2 and PNO-MP2 on gly_n chains ($n = 1, 2, 4, 8, 16$) in the cc-pVTZ basis set. The PNO-MP2 calculation has been carried out using a PNO threshold of $T_{PNO} = 10^{-8}$. For this comparison the time for the solution of he Z-CPHF equations has not been considered.

Concerning the accuracy, Tables 7 and 8 clearly show that PNO thresholds as loose as $T_{\mathrm{PNO}} = 10^{-6}$ do lead to unacceptable errors in geometries in almost all water clusters. This can be rationalised by the fact that the dispersion effect from weak pairs contributes substantially to hydrogen bonds. Apparently, the weak pairs needed for the description of hydrogen bonds are discarded at loose PNO thresholds which leads to the overestimation of intermolecular distances. Tightening the PNO threshold to 10^{-7} already yields a significant improvement for all water clusters and basis sets. The mean absolute errors in O–O distances fall below 2 pm. The MP2 intrinsic error also was found to be in the range of 2 pm for water clusters up to water hexamers. These errors were determined by comparing CCSD(T) to MP2 geometries [78]. Further lowering the PNO threshold does not lead to a significant decrease of errors in neighbour O–O distances.

The bond angles, however, still improve further with lower PNO thresholds of 10^{-8} or 10^{-9} when large basis sets are used. While in the aug-cc-pVTZ basis, the results for the bond angles change only little between $T_{\mathrm{PNO}} = 10^{-7}$ and $T_{\mathrm{PNO}} = 10^{-8}$, this is not yet the case in the aug-cc-pVQZ basis set. Especially for the water octamers, where the mean absolute error is still 3.4°–3.8° with $T_{\mathrm{PNO}} = 10^{-7}$. With a PNO threshold of 10^{-8}, the mean absolute errors drop below 0.7°. The maximum errors also decrease significantly, especially for the water octamers.

Since the maximum errors all occur in O–H···O and H···O–H(···O) angles, which are, compared to covalent bond angles, rather loose degrees of freedom, the accuracy achieved with $T_{\mathrm{PNO}} = 10^{-7}$ might already be sufficient. This might in particular be the case for the binding energies where the differences between MP2 and PNO–MP2 are already with $T_{\mathrm{PNO}} = 10^{-7}$ in all cases below 1 kcal/mol per hydrogen bond.

4.3. Performance of the implementation

To investigate the performance of the implementation, calculations on increasingly large glycine chains have been done. The wall times for the computation of the correlation contributions to the one- and two-particle densities are shown for canonical RI–MP2 and PNO–MP2 in Figure 5. At this point it should also be mentioned that the local RI approximation, which we do not yet exploit in our preliminary implementation, will lead to a further reduction of the scaling.

From Figure 5, it can be seen that canonical RI–MP2 and PNO–MP2 show a reasonably early break even point at approximately 1060 basis functions. The asymptotic scaling of canonical MP2 is in the order of $\mathcal{O}(\mathcal{N}^5)$

Table 9. Comparison of the PNO–MP2 and MP2 binding energies for different water clusters with and without CP-correction. The binding energies have been calculated at geometries optimised with the respective method/PNO threshold given in the second column.

		aug-cc-pVTZ		aug-cc-pVQZ	
		E_{int}	E_{int}^{CP}	E_{int}	E_{int}^{CP}
$(H_2O)_6$ (Prism)	$T_{PNO} = 10^{-6}$	−47.9	−44.0	−45.2	−43.3
	$T_{PNO} = 10^{-7}$	−50.0	−45.7	−48.6	−46.5
	$T_{PNO} = 10^{-8}$	−49.8	−45.6	−49.0	−46.9
	$T_{PNO} = 10^{-9}$	−49.7	−45.5	−49.0	−46.9
	MP2	−49.8	−45.6	−48.9	−46.8
$(H_2O)_6$ (Cage)	$T_{PNO} = 10^{-6}$	−47.7	−43.9	−44.9	−43.0
	$T_{PNO} = 10^{-7}$	−49.9	−45.6	−48.4	−46.3
	$T_{PNO} = 10^{-8}$	−49.7	−45.5	−48.9	−46.8
	$T_{PNO} = 10^{-9}$	−49.6	−45.4	−48.9	−46.8
	MP2	−49.7	−45.5	−48.9	−46.8
$(H_2O)_6$ (Book)	$T_{PNO} = 10^{-6}$	−47.3	−43.7	-[a]	-[a]
	$T_{PNO} = 10^{-7}$	−49.3	−45.2	−47.8	−45.8
	$T_{PNO} = 10^{-8}$	−49.4	−45.4	−48.5	−46.5
	$T_{PNO} = 10^{-9}$	−49.3	−45.2	−48.7	−46.7
	MP2	−49.4	−45.3	−48.6	−46.6
$(H_2O)_8$ (D_{2d})	$T_{PNO} = 10^{-6}$	−75.6	−69.5	−70.2	−67.3
	$T_{PNO} = 10^{-7}$	−79.5	−72.7	−77.0	−73.6
	$T_{PNO} = 10^{-8}$	−79.4	−72.6	−78.4	−75.0
	$T_{PNO} = 10^{-9}$	−79.3	−72.5	−78.0	−74.7
	MP2	−79.5	−72.6	−77.8	−74.5
$(H_2O)_8$ (S_4)	$T_{PNO} = 10^{-6}$	−75.7	−69.5	-[b]	-[b]
	$T_{PNO} = 10^{-7}$	−79.4	−72.6	−77.0	−73.6
	$T_{PNO} = 10^{-8}$	−79.4	−72.6	−78.5	−75.0
	$T_{PNO} = 10^{-9}$	−79.3	−72.4	−78.0	−74.7
	MP2	−79.5	−72.6	−77.8	−74.5

[a]No reasonable geometry found.
[b]No convergence achieved.

(the effective scaling obtained from a linear regression between 706 and 2650 basis functions is in the order of $\mathcal{O}(\mathcal{N}^{4.7})$). The scaling of our PNO–MP2 implementation, in contrast, is only in the order of $\mathcal{O}(\mathcal{N}^{3.2})$. Since our iterative PNO construction also shows a very similar scaling behaviour, this suggests that no additional bottleneck is introduced when computing the correlation contribution to the gradient.

Concerning the dependence of the efficiency on the PNO threshold, it should be noted that the computational costs increase quadratically with the number of PNOs per pair and linearly with the number of pairs.

5. Conclusions

We presented an implementation of the PNO–MP2 gradient. The equations have been derived by augmenting the canonical RI–MP2 Lagrangian with the localisation constraint and restricting the doubles amplitudes to the PNO space. A statistical analysis of the errors relative to canonical RI–MP2 demonstrates that the errors introduced by the PNO approximation are negligible with respect to the intrinsic error of the MP2 method. Geometry optimisations for water clusters of different size show that the errors are larger for weakly bound systems. Since also the intrinsic error of MP2 is larger for intermolecular distances and effects such as the BSSE increase the uncertainty, it can be stated that also here PNO thresholds of 10^{-7}–10^{-8} are sufficient to obtain accurate geometries.

The convergence may be improved in the future by including the PNO and OSV equations as additional constraints in the Lagrangian. Furthermore, the correction for neglected pairs and PNOs have not been considered in the preliminary implementation reported here. Whether these points will enhance the efficiency or merely increase the computational costs is subject of ongoing work.

Acknowledgments

Financial support from the Deutsche Forschungsgemeinschaft (DFG) through grant no. HA/2588/7 is gratefully acknowledged.

Disclosure statement

No potential conflict of interest was reported by the author(s).

Funding

This work was supported by the Deutsche Forschungsgemeinschaft (DFG) [grant number HA/2588/7].

References

[1] P. Pulay, Chem. Phys. Lett. **100**, 151 (1983).
[2] S. Saebø and P. Pulay, Chem. Phys. Lett. **113**, 13 (1985).
[3] S. Saebø and P. Pulay, Ann. Rev. Phys. Chem. **44**, 213 (1993).
[4] P. Pulay and S. Saebø, Theor. Chim. Acta **69**, 357 (1986).
[5] S. Saebø and P. Pulay, J. Chem. Phys. **86**, 914 (1987).
[6] S. Saebø and P. Pulay, J. Chem. Phys. **88**, 1884 (1988).
[7] G. Rauhut, P. Pulay, and H.J. Werner, J. Comput. Chem. **19**, 1241–1254 (1998).
[8] M. Schütz, G. Hetzer, and H.J. Werner, J. Chem. Phys. **111**, 5691 (1999).
[9] C. Hampel and H.J. Werner, J. Chem. Phys. **104**, 6286 (1996).
[10] M. Schütz, Phys. Chem. Chem. Phys. **4**, 3941 (2002).
[11] M. Schütz and F.R. Manby, Phys. Chem. Chem. Phys. **5**, 3349 (2003).
[12] G.D. Purvis and R.J. Bartlett, J. Chem. Phys. **76**, 1910 (1982).
[13] H.J. Werner and M. Schütz, J. Chem. Phys. **135**, 144116 (2011).
[14] M. Schütz, O. Masur, and D. Usvyat, J. Chem. Phys. **140**, 244107 (2014).
[15] K. Raghafavachari, G.W. Trucks, J.A. Pople, and M. Head-Gordon, Chem. Phys. Lett. **157**, 479 (1989).
[16] R.J. Bartlett, J.D. Watts, S.A. Kucharski, and J. Noga, Chem. Phys. Lett. **165**, 513 (1990).
[17] M. Schütz and H.J. Werner, J. Chem. Phys. **2000**, 9986 (2000).

[18] W. Meyer, *Methods of Electronic Structure Theory*, 3rd ed. (Plenum Press, New York, 1977).
[19] W. Meyer, Theor. Chem. Acc. **35**, 277 (1974).
[20] W. Meyer, J. Chem. Phys. **58**, 1017 (1973).
[21] W. Meyer, Int. J. Quantum. Chem. **S5**, 341 (1971).
[22] R. Ahlrichs, F. Driessler, H. Lischka, V. Staemmler, and W. Kutzelnigg, J. Chem. Phys. **62**, 1235 (1975).
[23] R. Ahlrichs and F. Driessler, Theor. Chem. Acc. **36**, 275 (1975).
[24] V. Staemmler and R. Jaquet, Theor. Chem. Acc. **59**, 487 (1981).
[25] J.L. Whitten, J. Chem. Phys. **58**, 4496 (1973).
[26] B.I. Dunlap, J.W.D. Conolly, and J.R. Sabin, J. Chem. Phys. **71**, 3396 (1973).
[27] F. Neese, A. Hansen, and D.G. Liakos, J. Chem. Phys. **131**, 064103 (2009).
[28] F. Neese, A. Hansen, and F. Wennmohs, S. Acc. Chem. Res. **42**, 641 (2009).
[29] F. Neese, F. Wennmohs, and A. Hansen, J. Chem. Phys. **130**, 114108 (2009).
[30] D.G. Liakos, A. Hansen, and F. Neese, J. Chem. Theory. Comput. **7**, 76 (2011).
[31] A. Hansen, D.G. Liakos, and F. Neese, J. Chem. Phys. **135**, 214102 (2011).
[32] C. Riplinger and F. Neese, J. Chem. Phys. **138**, 034106 (2013).
[33] J. Yang, G.K.L. Chan, F.R. Manby, M. Schütz, and H.J. Werner, J. Chem. Phys. **136**, 144105 (2012).
[34] C. Hättig, D.P. Tew, and B. Helmich, J. Chem. Phys. **136**(20), 204105 (2012).
[35] C. Krause and H.J. Werner, Phys. Chem. Chem. Phys. **14**, 7591 (2012).
[36] G. Schmitz, B. Helmich, and C. Hättig, Mol. Phys. **111**, 2463 (2013).
[37] B. Helmich and C. Hättig, J. Chem. Phys. (2013).
[38] B. Helmich and C. Hättig, Comput. Theor. Chem. **1040-1041**, 35–44 (2014).
[39] D.P. Tew and C. Hättig, Int. J. Quantum Chem. **113**(3) (2013).
[40] D.P. Tew and C. Hättig, J. Chem. Phys. **135**(7), 074107 (2011).
[41] G. Schmitz, C. Hättig, and D.P. Tew, Phys. Chem. Chem. Phys. **16** (2014).
[42] C. Riplinger, B. Sandhoefer, A. Hansen, and F. Neese, J. Chem. Phys. **139**, 134101 (2013).
[43] H.J. Werner, G. Knizia, C. Krause, M. Schwilk, and M. Dornbach, J. Chem. Theor. Comput. **11**, 484 (2015).
[44] Q. Ma and H.J. Werner, J. Chem. Theor. Comput. **11**, 5291 (2015).
[45] P. Pinski, C. Riplinger, E.F. Valeev, and F. Neese, J. Chem. Phys. **143**, 034108 (2015).
[46] C. Riplinger, P. Pinski, U. Becker, E.F. Valeev, and F. Neese, J. Chem. Phys. **144**, 024109 (2016).
[47] T. Helgaker, P. Jørgensen, and J. Olsen, *Molecular Electronic-Structure Theory* (Wiley, Chichester, 2000).
[48] C. Hättig, J. Chem. Phys. **118**(17), 7751 (2003).
[49] B. Helmich and C. Hättig, J. Chem. Phys. **135**(21), 214106 (2011).
[50] S.F. Boys, Rev. Mod. Phys. **32**, 296 (1960).
[51] N.C. Handy and H.F. Schaefer, J. Chem. Phys. **81**, 5031 (1984).
[52] M. Schütz, H.J. Werner, R. Lindh, and F.R. Manby, J. Chem. Phys. **121**, 737 (2004).
[53] F. Weigend, J. Comput. Chem. **30;29**(2), 167 (2008).
[54] C. Hättig, A. Hellweg, and A. Köhn, Phys. Chem. Chem. Phys. **8**, 1159 (2006).
[55] TURBOMOLE GmbH, *TURBOMOLE V7.1 2014, a development of University of Karlsruhe and Forschungszentrum Karlsruhe GmbH, 1989–2007, TURBOMOLE GmbH, since 2007; available from*http://www.turbomole. com. (Forschungszentrum Karlsruhe GmbH, Karlsruhe, 2014).
[56] F. Furche, R. Ahlrichs, C. Hättig, W. Klopper, M. Sierka, and F. Weigend, Wiley Interdisciplinary Reviews: Computational Molecular Science **4**(2), 91 (2014).
[57] M. v Arnim and R. Ahlrichs, J. Comput. Chem. **19**, 1746 (1998).
[58] M. Häser and R. Ahlrichs, J. Comput. Chem. **10**, 104 (1989).
[59] F. Weigend, Phys. Chem. Chem. Phys. **8**, 1057 (2006).
[60] F. Weigend, Phys. Chem. Chem. Phys. **4**, 4285 (2002).
[61] C. Hättig and F. Weigend, J. Chem. Phys. **113**, 5154 (2000).
[62] C. Hättig, A. Hellweg, and A. Köhn, Phys. Chem. Chem. Phys. **8**, 1159 (2006).
[63] A. Schäfer, H. Horn, and R. Ahlrichs, J. Chem. Phys. **97**, 2571 (1992).
[64] F. Weigend and R. Ahlrichs, Phys. Chem. Chem. Phys. **7**, 3297 (2005).
[65] F. Weigend, F. Furche, and R. Ahlrichs, J. Chem. Phys. **119**, 12753 (2003).
[66] T.H. Dunning Jr, ,J. Chem. Phys. **90**, 1007 (1989).
[67] R.A. Kendall, T.H. Dunning Jr, and R.J. Harrison, J. Chem. Phys. **96**, 6796–6806 (1992).
[68] D.E. Woon and T.H. Dunning Jr, ,J. Chem. Phys. **98**, 1358–1371 (1993).
[69] F. Weigend, A. Köhn, and C. Hättig, J. Chem. Phys. **116**(8), 3175 (2002).
[70] F. Weigend, M. Häser, H. Patzelt, and R. Ahlrichs, Chem. Phys. Lett. **294**, 143 (1998).
[71] J. Baker, J. Comput. Chem. **14**(9), 1085 (1993).
[72] K.L. Bak, J. Gauss, P. Jørgensen, J. Olsen, T. Helgaker, and J.F. Stanton, J. Chem. Phys. **6548**, 114 (2001).
[73] S. Coriani, D. Marchesan, J. Gauss, C. Hättig, T. Helgaker, and P. Jørgensen, J. Chem. Phys. **123**, 184107 (2005).
[74] C. Pérez, M.T. Muckle, D.P. Zaleski, N.A. Seifert, B. Temelso, G.C. Shields, Z. Kisiel, and B.H. Pate, Science **336**, 897 (2012).
[75] I.M.B. Nielsen, E.T. Seidl, and C.L. Janssen, J. Chem. Phys. **110**(19), 9435 (1999).
[76] M. Schütz, H.J. Werner, R. Lindh, and F.R. Manby, J. Chem. Phys. **121**(2), 737 (2004).
[77] S. Boys and F. Bernadi, Mol. Phys. **19**, 553 (1970).
[78] E. Miliordos, E. Aprà, and S.S. Xantheas, J. Chem. Phys. **139**, 114302 (2013).